Order Number 1345427

Room-temperature carrier lifetimes and optical nonlinearities of GaInAs/AlInAs and GaAlInAs/AlInAs MQW devices at 1.3μm

Johns, Steven T., M.S.

The University of Arizona, 1991

U·M·I
300 N. Zeeb Rd.
Ann Arbor, MI 48106

Room-Temperature Carrier Lifetimes and Optical Nonlinearities of GaInAs/AlInAs and GaAlInAs/AlInAs MQW Devices at 1.3μm

by

Steven Johns

A Thesis Submitted to the Faculty of the

OPTICAL SCIENCES CENTER

In Partial Fulfillment of the Requirements
for the Degree of

MASTER OF SCIENCE

In the Graduate College of

THE UNIVERSITY OF ARIZONA

1 9 9 1

STATEMENT BY AUTHOR

This thesis has been submitted in partial fulfillment of the requirements for an advanced degree at The University of Arizona and is deposited in the University Library to be made available to borrowers under rules of the library.

Brief quotations from this thesis are allowable without special permission, provided that accurate acknowledgment of source are made. Requests for permission for extended quotation from or reproduction of this manuscript in whole or in part may be granted by the head of the major department or the Dean of the Graduate College when in his or her judgement the proposed use of the material is in the interest of scholarship. In all other instances, however, permission must be obtained from the author.

SIGNED: Steven T Lahse

APPROVAL BY THESIS DIRECTOR

This thesis has been approved on the date shown below:

Nasser Peyghambarian
Professor, Optical Sciences

7/19/91
Date

to my wife lori and children lindsay and nicholas

ACKNOWLEDGMENTS

For his hard work and dedication on the exciton saturation measurements, I would like to express all my gratitude to Chia Chen Hsu. I would also like to thank Jason Sokoloff and Brian McGinnis for useful discussions on theoretical and experimental procedures. The guidance of Nasser Peyghambarian was essential for this work. I would like to thank Hyatt Gibbs and Galina Khitrova for the supply of MQW and etalon samples used in this thesis.

I would like to thank Mark Krol, for without his assistance this experiment would have been far more difficult to perform. Also for technical discussions, I would like to thank Lt. Ed Toughlian and Ray Boncek. I am also grateful to John Stacy, who initiated this work with Nasser.

I would like to thank all my supervisors at Rome Laboratories who allowed me to participate in the Long Term Full Time Study Program. If a program such as this didn't exist I would not be receiving my degree today. Thank you.

TABLE OF CONTENTS

LIST OF ILLUSTRATIONS

LIST OF TABLES

ABSTRACT

The room-temperature nonlinear absorption spectra of a GaInAs/AlInAs and a GaAlInAs/AlInAs multiple quantum well (MQW) were measured near 1.3 μm using a pump-probe technique. Saturation carrier densities at the heavy-hole exciton peak were determined to be 1.2 x 10^{18} and 1.0 x 10^{18} cm^{-3} with carrier lifetimes of $\simeq$ 2.3 ns and $\simeq$ 750 ps for the two samples, respectively. Fabry-Perot etalons with integrated mirrors grown by molecular beam epitaxy (MBE) with GaInAs/AlInAs MQWs as spacer layers were also fabricated as optical switching devices. A 175 ps recovery time was measured for the etalon at room temperature.

1.0 INTRODUCTION

The use of optics in communication systems has opened the door for the development of high bit-rate Local Area Networks (LANs). Multiple gigabit LAN architectures have been proposed over the past few years. These multiple gigabit systems are not feasible with electronic components due to their speed limitations. Thus, a significant amount of research is being conducted to replace these electronic components with optical devices. By doing so the speeds and bandwidth of communication systems can be greatly increased.

In present state-of-the-art communication systems, data are transmitted over optical fibers because of their low-loss and low-dispersion properties. All switching and/or signal processing operations must be carried out electronically, therefore an opto-electronic conversion must take place. These conversions add to switching complexities and limit overall system speed. Optical devices offer the potential to eliminate or significantly reduce the limitations imposed by electronic interfaces.

Various Optical Time Division Multiple Access (OTDMA) architectures have been proposed over the past few years[Tucker et al. (1988),Pruncnal et al. (1990)]. In an

OTDMA, very low bit-rate data streams are time-multiplexed to create a high bit-rate data stream. These high bit-rate data streams utilize a greater portion of the available bandwidth of an optical fiber. For detection and conversion into the electrical domain, the data stream must be demultiplexed into several low rate channels. In general, high bit-rate systems place a great demand on the interface components' ability to switch optical signals at high speeds. For 10 Gbit/sec systems, optical switches with large switching ratios and full recovery within 100 picoseconds are needed to fulfill the OTDMA requirements. In this thesis, nonlinear Fabry-Perot etalons are being studied as a possible solution to this problem.

Semiconductor Fabry-Perot etalons have been used to demonstrate optical switching as well as other logic-gate applications. Most of the research has concentrated on devices operating at .83 μm and 1.5 μm wavelength[Tai et al. (1987), Lee et al. (1986), Migus et al. (1985)]. Because of the vast applications of 1.3 μm wavelength light in fiber communication systems, this research has focused on the demonstration of switching in etalons at 1.3 μm. The materials to be reported on here are GaInAs/AlInAs and GaAlInAs/AlInAs multiple-quantum-well devices.

2.0 FABRY-PEROT ETALON

A Fabry-Perot etalon consists of two partially reflective parallel plates separated by a medium of thickness d and index of refraction n. As in Figure 2.1, an incident electric field with amplitude A is partially reflected (A_{1r}) and partially refracted (A'_{1t}). The refracted field travels

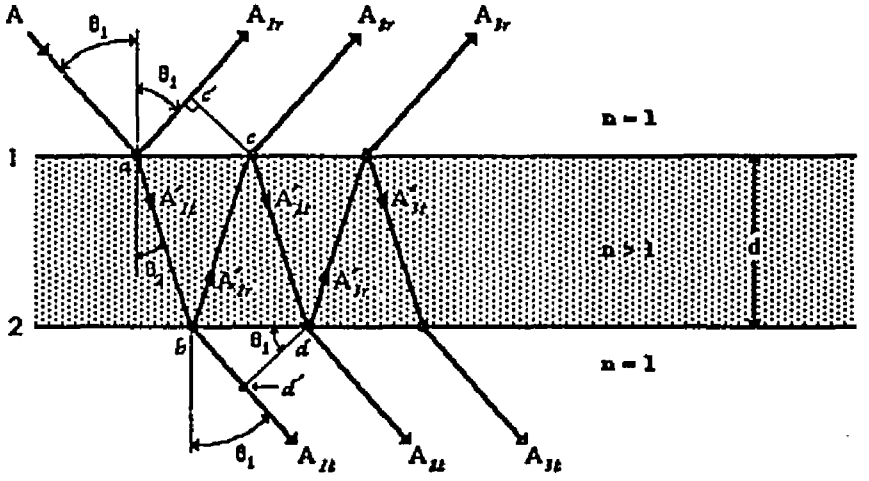

Figure 2.1 - Multpile Beam Interference in Nonabsorbing Fabry-Perot Etalon.

through the plate where it is again reflected (A'_{2r}) and refracted (A_{1t}). The reflected wave travels back towards the first surface where again it gets reflected (A'_{2t}) and refracted (A_{2r}). Multiple reflections and refractions take place for a single input field.

When the transmitted fields A_{1t}, A_{2t} ...A_{Nt} are summed at the output of the plate, the phase difference between the fields must be calculated. For cavity length d, the optical path difference $n\delta$ between A_{mt} and $A_{(m+1)t}$ is given by:

$$n\delta = 2ndCos(\theta_2) \qquad (1)$$

Where θ_2 is the angle of the refracted field with respect to the normal of the surface. Reflections at the surfaces could cause phase shifts to the incident fields. In this case, the only reflection that one must be concerned about is the initial reflection from the first surface. The rest of the reflections, which are due to the plate/air interface will introduce the same amount of phase shift for even number of reflections as well as for odd number of reflections. Therefore all the transmitted fields and all the reflected fields (N > 1) will have the same change of phase due to reflections. Since the plate has index n, the phase difference due to the path difference traveled for each pass is given by $2\pi(n\Delta/\lambda_o)$, where Δ is the phase and λ_o is the free space wavelength. The phase Δ for the transmitted fields is:

$$\Delta = \frac{2\pi n\delta}{\lambda_o} = \frac{4\pi ndCos(\theta_2)}{\lambda_o} \qquad (2)$$

The total field of the reflected or transmitted wave is found by summing all the fields emerging for each surface. Assuming the relationships $tt' = 1 - r^2$ and $r' = -r$, where t and r are transmission and reflection coefficients, respectively, the total transmitted amplitude field A_t is:

$$A_t = A\left[\frac{1-R}{1-Re^{i\Delta}}\right] \tag{3}$$

Where $R = |r|^2$ and is defined to be the reflectance of the surfaces. Multiplying equation 3 by its complex conjugate A^*_t and dividing by the incident intensity I_i, results in a normalized expression for the intensity of the transmitted fields I_t:

$$\frac{I_t}{I_i} = \frac{1}{1+FSin^2\left(\frac{\Delta}{2}\right)} \tag{4}$$

where

$$F = \frac{4R}{(1-R)^2}. \tag{5}$$

The term F is defined to be the *coefficient of finesse* of the cavity. Also the medium is assumed to have no absorption, therefore $I_t + I_r = I_i$. In this case, there is no loss of energy in the system. The case where absorption is present within the etalon will be considered later.

Assuming that the incident light is perpendicular to the incident surface, it is seen from equation 4 that peak transmission through the etalon occurs when Δ is an even multiple of π. Transmission approaches unity due to constructive interference of the transmitted components. Maximum reflection occurs when Δ is an odd multiple of π, and is due to destructive interference. The special case of maximum transmission is called the *resonance condition*. The two reflective surfaces create a resonant cavity resulting in the modulation of transmission as a function of Δ. As seen in Figure 2.2, these peaks repeat every time the phase condition for maximum transmission is meet. Also, the sharpness of these peaks is a function of the reflectivity of the surfaces. The closer the reflectivity is to unity, the sharper the peaks will be as seen in equation 5.

For the case when the medium has some absorption the effect on the transmitted signal is seen as an attenuation of the peaks. Since in general the absorption is a function of wavelength, the resonant peaks will be attenuated as a function of wavelength. The etalon characteristics now become dependent on absorbed energy, wavelength of operation and induced carrier densities, which make the device model much more difficult to describe and understand, but also makes it useful as an all-optical switch.

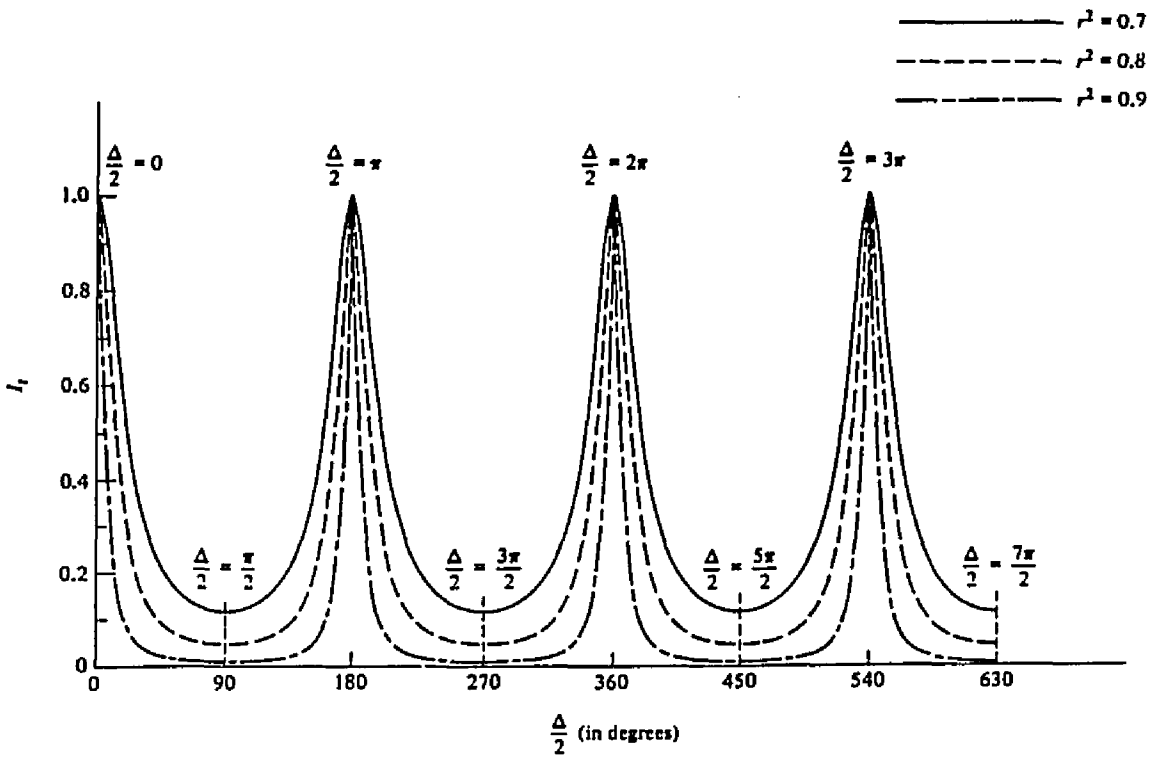

Figure 2.2 - Transmission of an Etalon as a Function of Phase and Reflectivity.

2.1 The Etalon as a Switching Element

The Fabry-Perot etalon can be used as a switching element in an optical system. The index of the etalon's medium can be changed by the absorption of light due to the generation of photo carriers. The change in index will

cause a change in optical path length which will change the resonant conditions inside the etalon. For a given wavelength just below a transmission peak which has initially low transmission, the shift in the peak would increase the transmission intensity of this wavelength. One could then optically control (via a controlling beam) the transmission of a specific wavelength by changing the intensity of light incident on the etalon.

As a way to modulate the index, semiconductor materials with nonlinear properties are used as the spacer in an etalon. The material's absorption characteristics, which are wavelength dependent, determine the index characteristics of the etalon. Absorbed incident light will cause changes in the index of the material. The amount of index change depends on the intensity and the wavelength of the incident light. By choosing materials which have large nonlinear optical properties, the refractive index of the material can be modulated and thus shift the position of the etalon's resonant peaks. The amount of shift in peak transmission is proportional to the change in index, as in equation 2.

Consider an ideal semiconductor with a step absorption spectrum where the step occurs at wavelength λ_o. That is, for $\lambda > \lambda_o$ no light is absorbed, and for $\lambda < \lambda_o$ light is

absorbed as shown in Figure 2.3. Also assume that the change in index at resonant wavelength λ_1 due to the absorbed light is linear. In order to make a switching

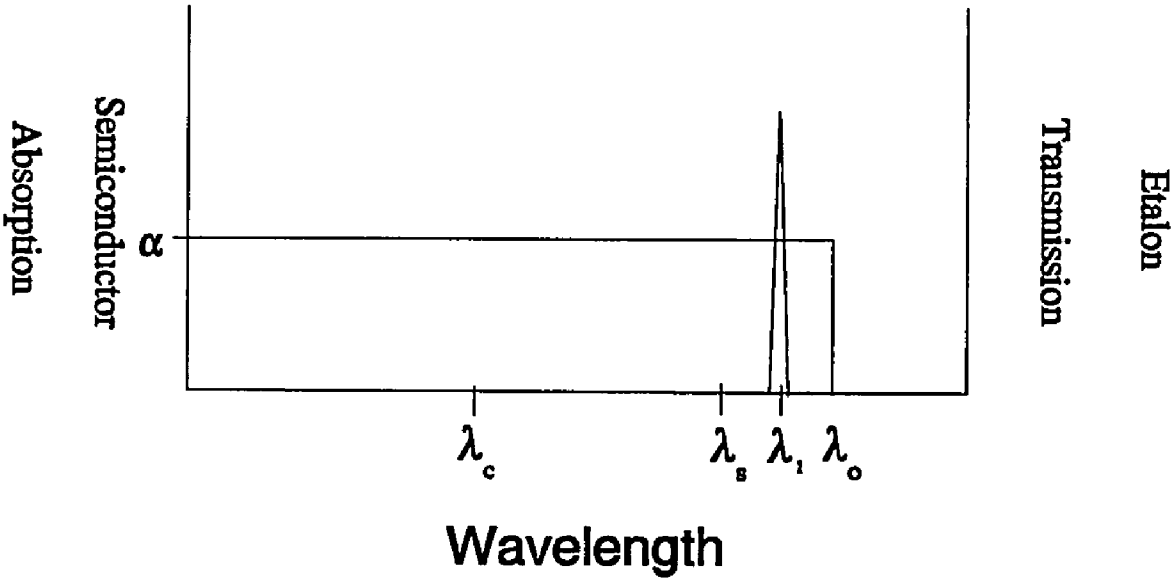

Figure 2.3 - Step Absorption and Etalon Transmission.

element, an etalon must be designed such that its coefficient of finesse is very high and that a peak transmission occurs at some wavelength below the absorption edge of the medium. By using two beams of different wavelengths, one to be absorbed by the medium (controller beam) and the other to monitor the change in the transmission (signal beam), the characteristics of the etalon can be measured.

The operation of the etalon as a switch is as follows. Choose a controlling beam wavelength λ_c to be less than λ_o. This beam will be absorbed by the medium and induce carriers which will change the index of the medium. Assuming that a very narrow resonant peak occurs at λ_1, choose a signal wavelength λ_s just below λ_1 which has no transmission due to the resonant conditions in the etalon. By modulating the intensity of the controlling beam λ_c, the transmission of the signal beam λ_s can be varied. Monitoring λ_s as a function of λ_c will characterize the switching of the etalon.

The nonlinear mechanisms which cause the change of index are the screening effect and bandfilling effects. When a large number of electron-hole pairs are created in a semiconductor due to high intensity laser light, the Coulomb potential is screened. This screening causes the excitonic resonances (as described in Section 3) to disappear at some crucial density thus changing the index of the material. Also as more electron-hole pairs are generated bandfilling occurs which results in a bleaching of the absorption in the vinicity of the bandedge. This bleaching appears as a shift of the bandedge to shorter wavelengths. When materials with nonlinearities are used as the active element of the etalon, both bandfilling and screening attribute to the change in

index which cause the etalon the shift the position of its fringes. A switching element is produced by controlling the transmission through an etalon by shifting is fringes as a function of incident light.

For an actual device, the explanation of the operating characteristics is significantly more complicated. For example, parameters such as switching speeds (turn-on times), carrier relaxation times (turn-off) and contrast ratio are dependent on several different parameters, such as shape of bandedge, wavelength of bandedge and reflectivity of integrated mirrors. For the types of devices studied here, the relaxation time is the main subject of our research.

3.0 MULTIPLE-QUANTUM-WELLS (MQWs)

A MQW is a periodic structure of alternating narrow and large bandgap semiconductors. The large bandgap semiconductors act as potential barriers which confine electrons to the narrow bandgap regions. The confinement of carriers in the well results in an absorption spectrum which has a staircase structure as shown in Figure 3.1. The bandedge position of the MQWs can be adjusted over a

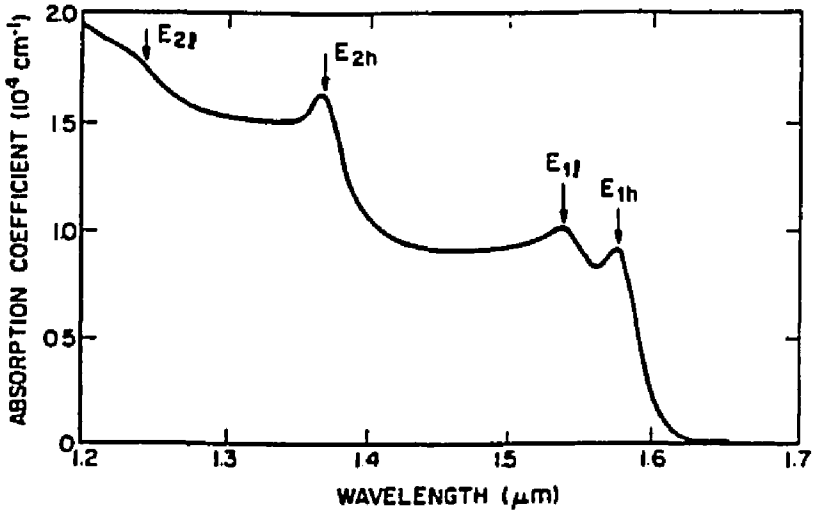

Figure 3.1 - Typical Shape of Room-Temperature Absorption Spectrum for MQWs.

specific wavelength region during the growth process by varying the well thickness. As a result, the absorption characteristics can be shifted in wavelength allowing device designs which fit a specific source spectrum and are no

longer limited to a fixed spectral band set by the bulk material bandgap.

Optical properties of bulk semiconductors at room temperature have been extensively studied for possible applications in fast optical systems. Materials such as bulk GaAs, InGaAs and InP exhibit large nonlinear behavior when high power optical pulses with wavelengths near the bandedge are incident on them. In MQW materials, large nonlinearities exist at room temperature due to presence of exciton absorption. For this reason, much theoretical and experimental research has been done to understand the optical properties of MQWs. Emphasis on the near infra-red region (.8-1.6μm) has driven the main thrust of research due to its vast applications in the communication field.

3.1 Properties of MQW's

In bulk materials, the absorption consists of two components: 1) the discrete excitonic transitions and 2)the band-to-band continuum. At room temperature, the excitonic transitions are broadened by phonon interaction, causing the absorption to exhibit an abrupt edge. As reported by [Park et al. (1988)], the bulk nonlinearities are smaller as compared to the nonlinearities of the MQWs. I n M Q W

materials, the room-temperature absorption spectra consists of well resolved excitonic resonances which are close to the bandedge, as seen in Figure 3.1.

GaAs MQWs have been extensively studied over the past decade and are considered to be well characterized. Comparisons of bulk and MQW structures have been made to further understand how each material can be used for device applications. A systematic study of the effect of well width on MQW properties as compared to bulk samples was performed [Park et al. (1988)]. The difference between bulk materials and MQWs is due to the confinement of electron-hole pairs in MQWs, which enhances the exciton absorption as the MQW well width is decreased. Figure 3.2 shows the absorption spectrum for several well widths as well as for bulk material. As discussed by Park, the maximum change in the refractive index is greatest for the smallest well size. One can then conclude that a nonlinear etalon made with small well widths MQWs should have the greatest shift in resonant peaks which could lead to large switching ratios. Since a strong exciton absorption line can be seen at room temperature, MQW devices make system applications more realistic. Experiments show that exciton saturation occurs on the picosecond time scale [Lambsdorff et al.(1991)], however, the recovery of excess carriers in MQWs is on the

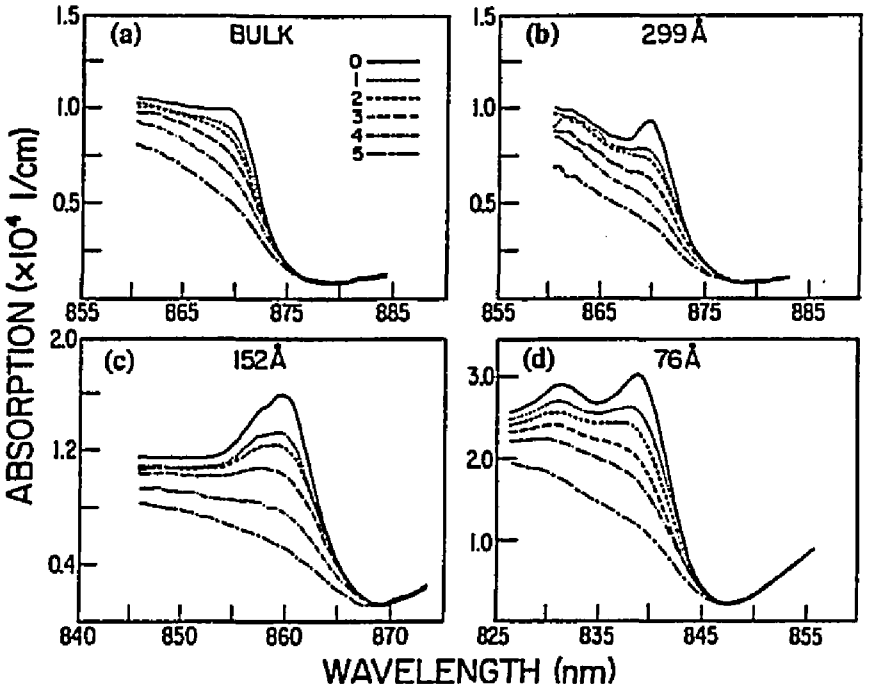

Figure 3.2 - Absorption Spectrum for GaAs MQWs as a Function of Well Width.

order of nanoseconds.

The most important parameter, as far as device speeds are concerned is the carrier recombination time. The recombination time of semiconductors limit the speed at which devices can be operated. For fast optical systems discussed earlier, it is desirable to have a recovery time on the order of 100 picoseconds. Recovery times for GaAs samples have been reported [Gibbs et al. 1990)] to be between 1 and 25 ns. Other reports claim recovery times as fast as 0.5 picoseconds as a result of proton-bombardment

processing[Lambsdorff et al. (1991), Silberberg et al. (1985)]. However, in these proton-bombarded samples optical degradation was also reported.

3.2 GaInAs and GaAlInAs Samples

Samples used in the experiment were $Ga_{0.47}In_{0.53}As/Al_{0.48}In_{0.52}As$ and $Ga_{0.376}Al_{0.094}In_{0.53}As/Al_{0.48}In_{0.52}As$ MQWs. Detailed growth conditions are described elsewhere by [Khitrova et al. (1991)]. The GaInAs/AlInAs MQW was grown with 100 periods of 40 Å GaInAs wells and 68 Å AlInAs barriers. A GaAlInAs/AlInAs MQW consisting of 100 periods of 90 Å GaAlInAs wells and 69 Å AlInAs barriers was also produced. As seen in Figure 3.3, both MQWs exhibit strong exciton absorption peaks at room temperature. The half-width of the lowest exciton peak was 14 mev for the GaInAs MQW and 12 mev for the GaAlInAs MQW. The position of these peaks can be tailored to some extent by design and growth parameters. In the ternary system, the transition energy of the exciton can be adjusted mainly by changing the quantun well thickness. For the quaternary system, both the well thickness and Ga:Al ratio can be used to shift the exciton absorption peak. The latter affords the opportunity to tailor other parameters such as the carrier lifetime or

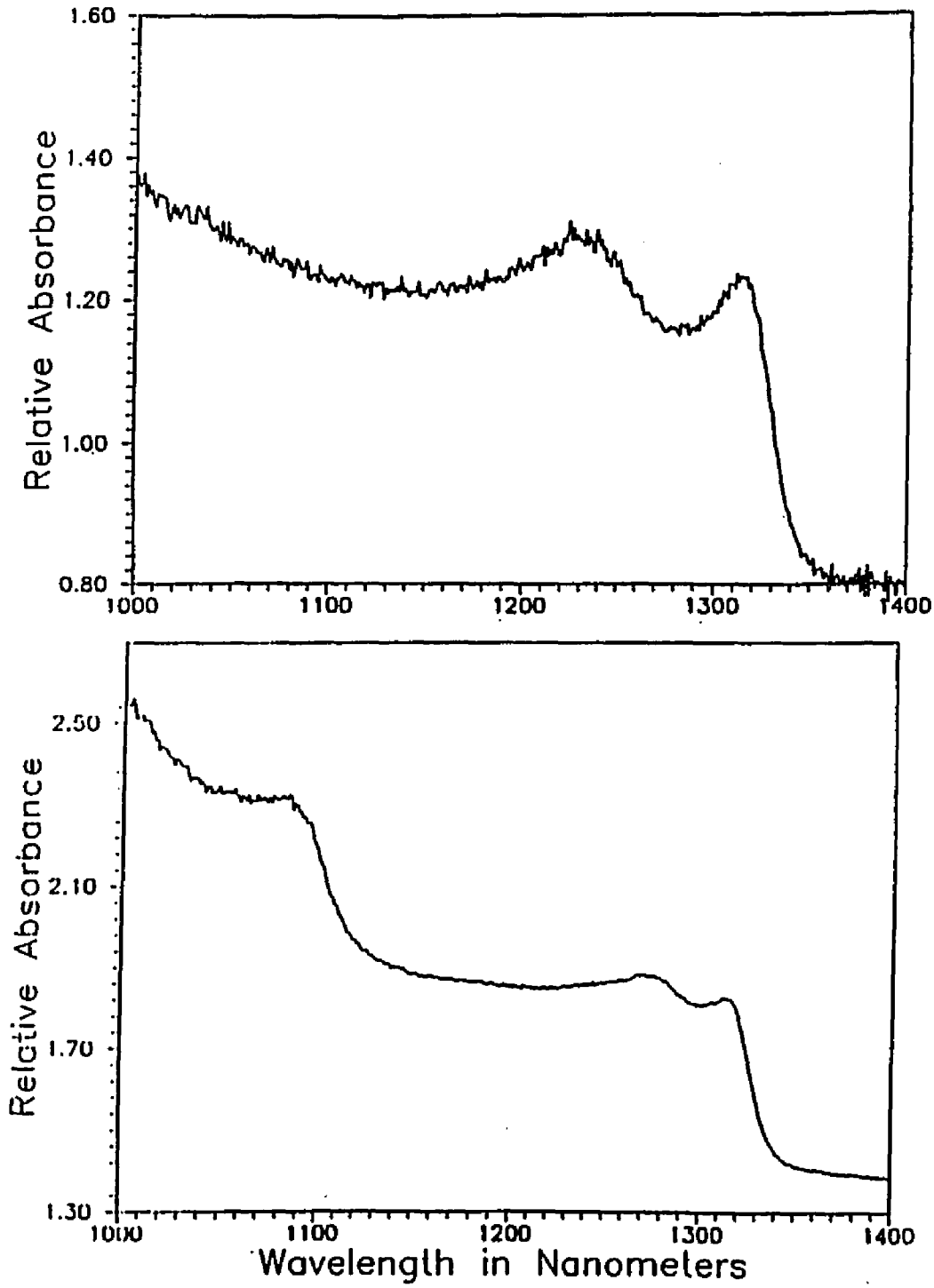

Figure 3.3 - White Light Absorption Spectrum for a) GaInAs and b) GaAlInAs MQWs.

exciton sharpness while maintaining the exciton at the same wavelength.

A Fabry-Perot etalon which has MBE-grown integrated mirrors was also fabricated. The design and growth parameters are described by [Khitrova et al. (1991)]. The etalon spacer consisted of 108 periods of GaInAs/AlInAs MQWs (35 Å wells and 58 Å barriers) with integrated high

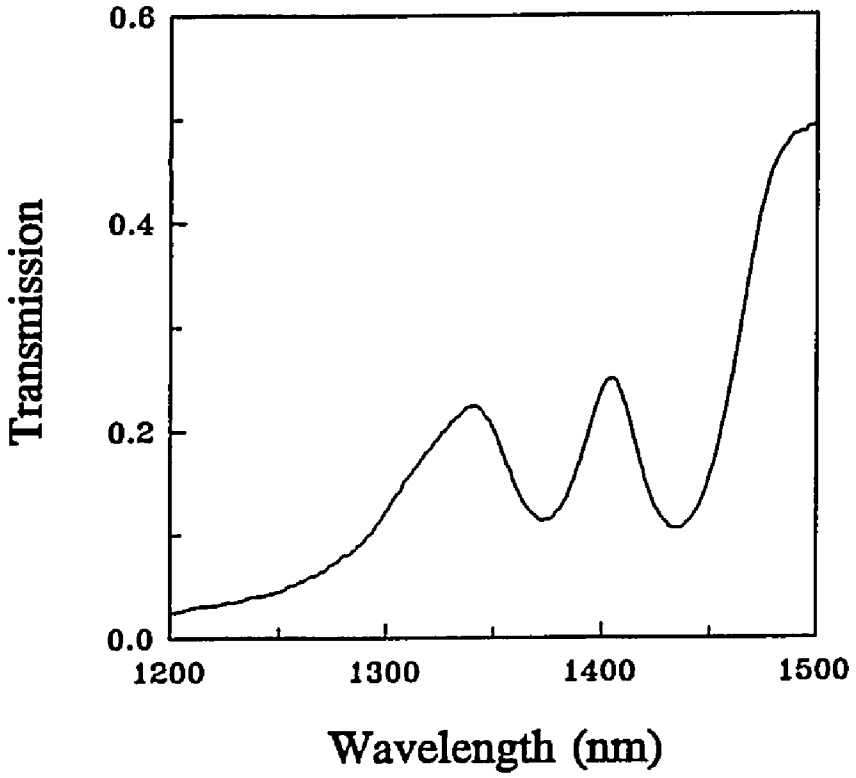

Figure 3.4 - White Light Transmission Spectrum for GaInAs Etalon.

reflectance mirrors. The mirrors were obtained by growing $\lambda/4$ layers of alternating high (GaAlInAs) and low (AlInAs) index materials. Figure 3.4 shows the spectra for the

etalon. The Ga:Al ratio was made low enough so the mirrors were non-absorbing at 1.3 μm. Since there was such a small difference in index, a large number of $\lambda/4$ layers had to be grown to achieve high reflectivity. By removing the InP substrate the reflectivity of the front and back mirrors became approximatively the same.

4.0 CHARACTERIZATION OF MQWs SAMPLES

Material characteristics, such as room temperature absorption spectrum, exciton saturation density and carrier lifetimes times of GaInAs/AlInAs, GaAlInAs/AlInAs MQWs and GaInAs/AlInAs etalons have been measured and the results are reported in the following sections.

4.1 Short Pulse Testing

In this experiment, short optical pulses were used to measure the switching characteristics of the two MQWs and one MQW etalon described in section 3.2. Results indicate that the measurements may be pulse limited as far as turn-on time is concerned, but that the recovery measurements could be accurately measured.

The fast response measurements of MQWs and MQW etalons is a good measure of the overall performance characteristics of the device. As discussed earlier, the recovery time of the device is the most important factor in determining the speed at which these devices can be operated. Measurement of these characteristics are performed with optical pulses in a time resolved pump-probe set-up. In this experiment, a high powered pump beam is used to create excess carriers

which change the absorption characteristics of the sample. Also a weak probe beam, which does not appreciably affect the sample's characteristics, is used to monitor the changes caused by the pump. In a time resolved measurement, the time delay between the pump and probe pulses is varied. Holding the probe fixed in time, the time delay of the pump is swept so that the pump goes from lagging the probe to leading the probe. When the pump is lagging the probe, the transmission of the probe is not affected by the pump. On the other hand, when the pump leads the probe the transmission of the probe becomes dependent on the effects caused by the pump intensity. These time resolved experiments are used to measure the switching speeds (turn-on) and the carrier recovery times (turn-off) of the samples.

For the GaInAs/AlInAs and GaAlInAs/AlInAs MQWs and the GaInAs/AlInAs Fabry-Perot etalon response measurements were performed using a time resolved pump-probe set-up. The laser source used was a Quantronix 416 Nd:YAG operating at 1.3 μm. This set-up is illustrated in Figure 4.1. The laser emits pulses of 125 picosecond (ps) in width (FWHM) at a rep-rate of 100 MHz. A fiber-grating compression system was used to obtain 2 ps pulses for use in the pump-probe experiments.

The compression system consists of 1.7 km of dispersion shifted fiber with zero wavelength dispersion at 1.55 μm and a pair of 1200 lines/mm diffraction gratings. The fiber produces a linear frequency chirp of 3.5 nm which was

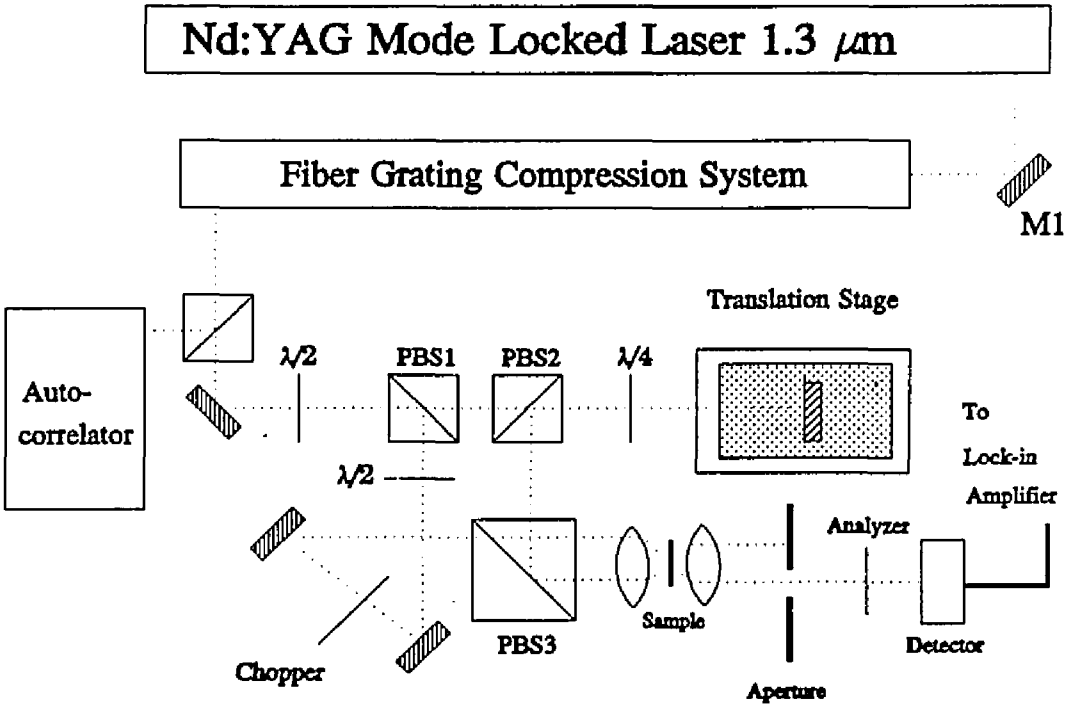

Figure 4.1 - Short Pulse Pump-Probe Experiment System.

compensated for with a grating dispersive delay line in a double pass configuration. Figure 4.2 shows an autocorrelator trace of 2 picosecond pulses produced by the pulse compression system. Further information on the pulse compression system is described by [Sokoloff et al. (1990)].

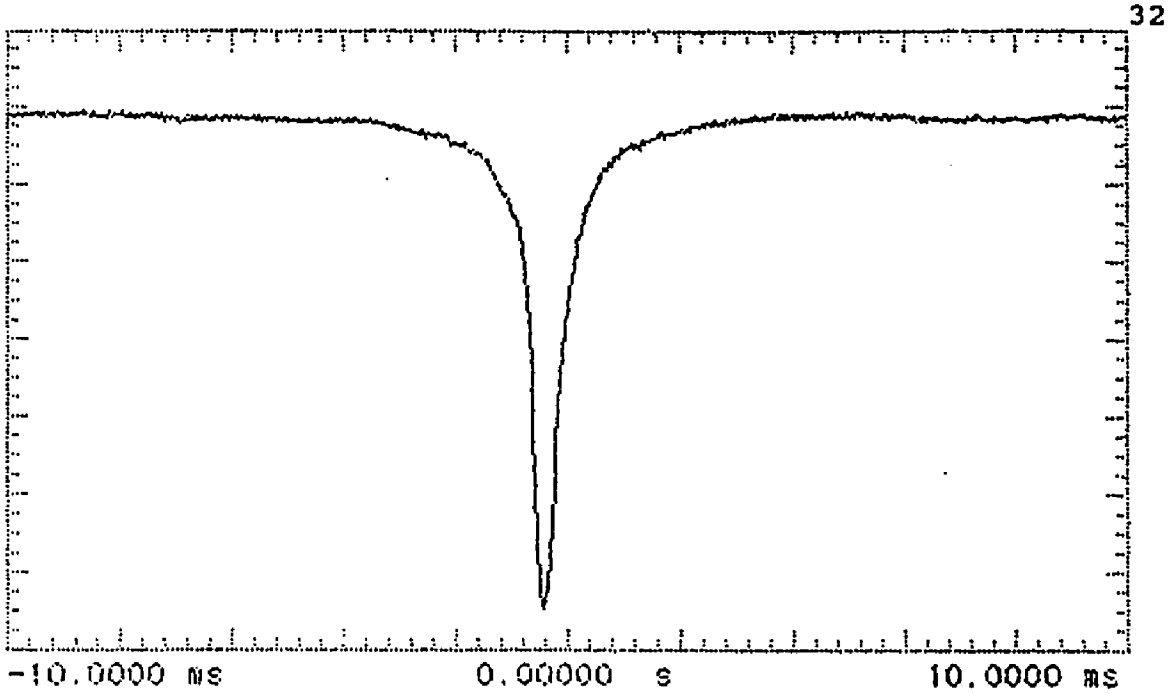

Figure 4.2 - Autocorrelation Trace of 2 Picosecond Pulses at 1.3 μm.

Time resolved measurements were performed using a pump-probe set-up as shown in Figure 4.1. At the input to the set-up is a $\lambda/2$ plate which can adjust the intensity ratio between the pump and probe beams after the first polarizing beam splitter (PBS1). The pump arm is then passed through a $\lambda/4$ plate and is retroreflected back on itself. The retroreflecting mirror is mounted on a translation stage which introduces the variable time delay between the pump and probe. This combination of $\lambda/4$ plate, mirror and $\lambda/4$ plate rotates the polarization 90° which allows for the separation of the rotated beam traveling in opposite direction by PBS2. In the probe arm the beam is passed through a $\lambda/2$ plate and the appropriate amount of delay to

match the delay in the pump arm. The delay is such that when the translation stage is at its center, the time difference between pump and probe is zero. The $\lambda/2$ plate is used to adjust the intensity of the probe beam after PBS3. The pump and probe beams are then recombined at PBS3 where they are orthogonally polarized but spatially separated. Using a 10x objective the two beams are co-focused onto the sample. The two beams are then recolliminated with a 10x objective and then the pump is blocked by an aperture. The probe beam is passed through an analyzer to isolate the probe from any scattering from the pump. A computer controls the stepper stage and records the voltages measured from the lock-in detection system.

Time resolved measurements were made by sweeping the delay between the pump and probe using a translation stage. Total travel of the stage limited measurements to 500 ps of time delay between the pump and probe. By chopping the probe beam, a lock-in amplifier was used to detect changes in transmission caused by the pump intensity.

Since the MQWs were designed to have an exciton absorption peak around 1.319 um, it was possible to carry out the pump-probe experiments with a single source at 1.319 μm. At this wavelength, the exciton absorption generates

sufficient excess carriers to induce nonlinearities in the sample.

The switching speeds of the GaInAs and GaAlInAs MQWs and GaInAs etalon were performed using the system described above. Pulses of 2 picosecond width were co-focused to a 26 μm diameter spot size on the sample. The translation stage varied the pump-probe delay from -50 ps to +50 ps with several data points taken at half picosecond increments. The calculated excess carrier density induced by a pump pulse of 20 mW was 1.5 x 10^{18} cm^{-3} for the GaInAs 40 Å MQW. In the GaAlInAs 90 Å MQW the carrier density was 1.7 x 10^{18} cm^{-3} for the same intensity. Table 4.1 lists all the calculated carrier densities for all pump powers used in the experiment.

The results from the switching experiments are shown in Figure 4.3. The best switching ratio for MQWs was 2:1. In both MQW samples, large preswitching can be seen at all pump powers. This is believed to be a function of the detection system which is caused by scattering of the pump into the probe. Also it seems that for the 40 Å GaInAs MQW, that this device does not fully recover for the 10 ns rep-rate of the laser. Since all the curves do not converge to the same starting level for negative time delay, the sample does not fully recover from the previous pump pulse. In the 90 Å

Table 4.1 - Photo-Generated Carrier Density for GaInAs and GaAlInAs MQWs

	GaInAs	GaAlInAs
Pump Intensity	Carrier Density	Carrier Density
mW	cm^{-3}	cm^{-3}
80	$5.9x10^{18}$	$6.7x10^{18}$
40	$2.9x10^{18}$	$3.4x10^{18}$
20	$1.5x10^{18}$	$1.7x10^{18}$
10	$7.3x10^{17}$	$8.4x10^{17}$
5	$3.7x10^{17}$	$4.2x10^{17}$
2	$1.5x10^{17}$	$1.7x10^{17}$

GaAlInAs MQW the levels for negative time delay seem to converge to a fixed level which shows that the sample fully recovers within the 10 ns rep-rate.

Figure 4.4 shows the switching results for the GaInAs etalon. In Figure 4.4 (a), three pump powers illustrate the switching contrast of the etalon. As shown here, the measured switching speed of the etalon is typically 4-5 ps. Since the pump and probe pulses used in this work were only 2 ps in duration, the switching speed could be pulse limited. Also in Figure 4.4 (b), additional curves for higher pump powers are plotted. As the power is increased above 20 mW, the level for negative time delay seems to decrease in transmission. This result could be explained as

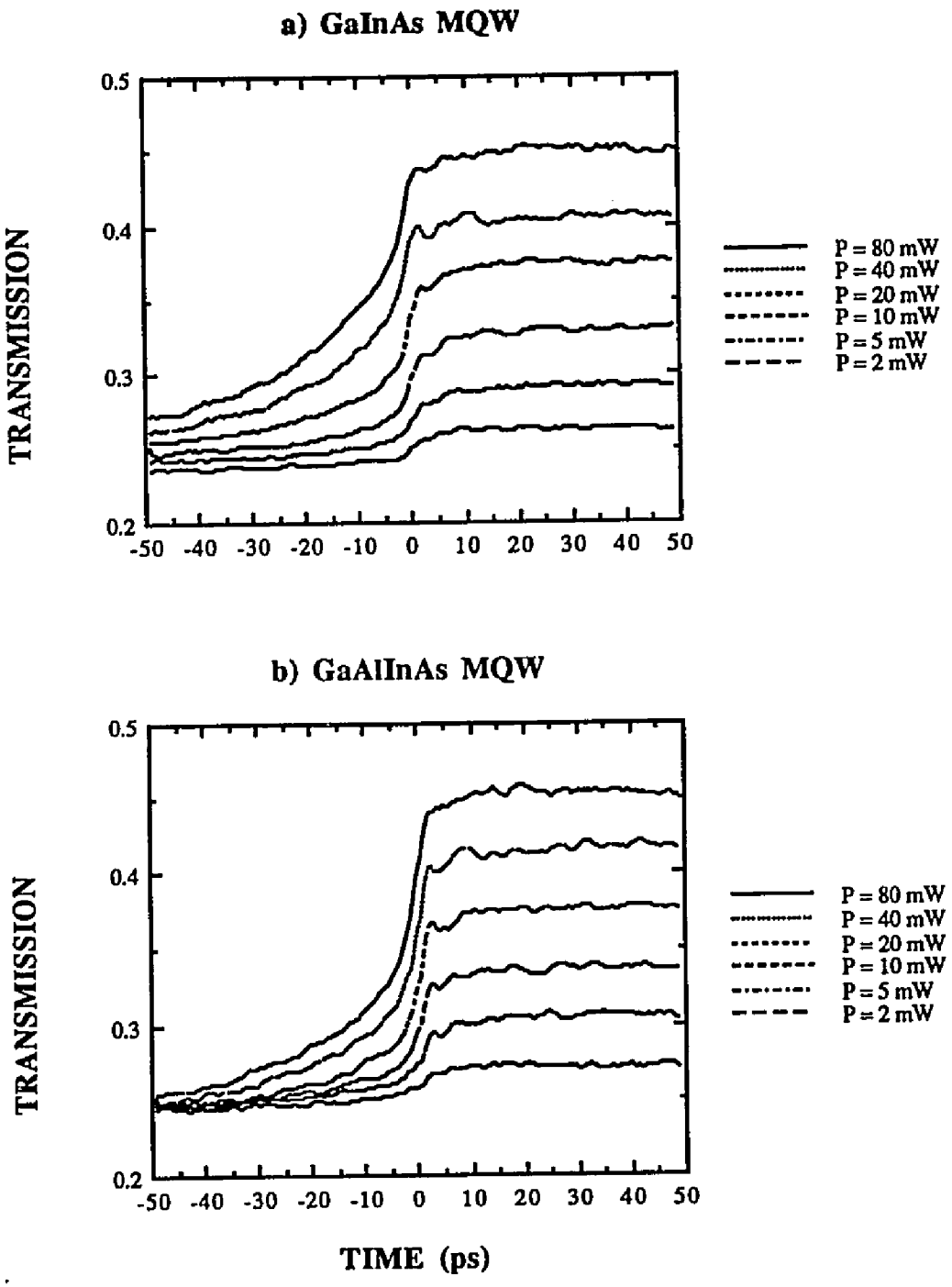

Figure 4.3 - Switching Characteristics for a) GaInAs and b) GaAlInAs MQWs.

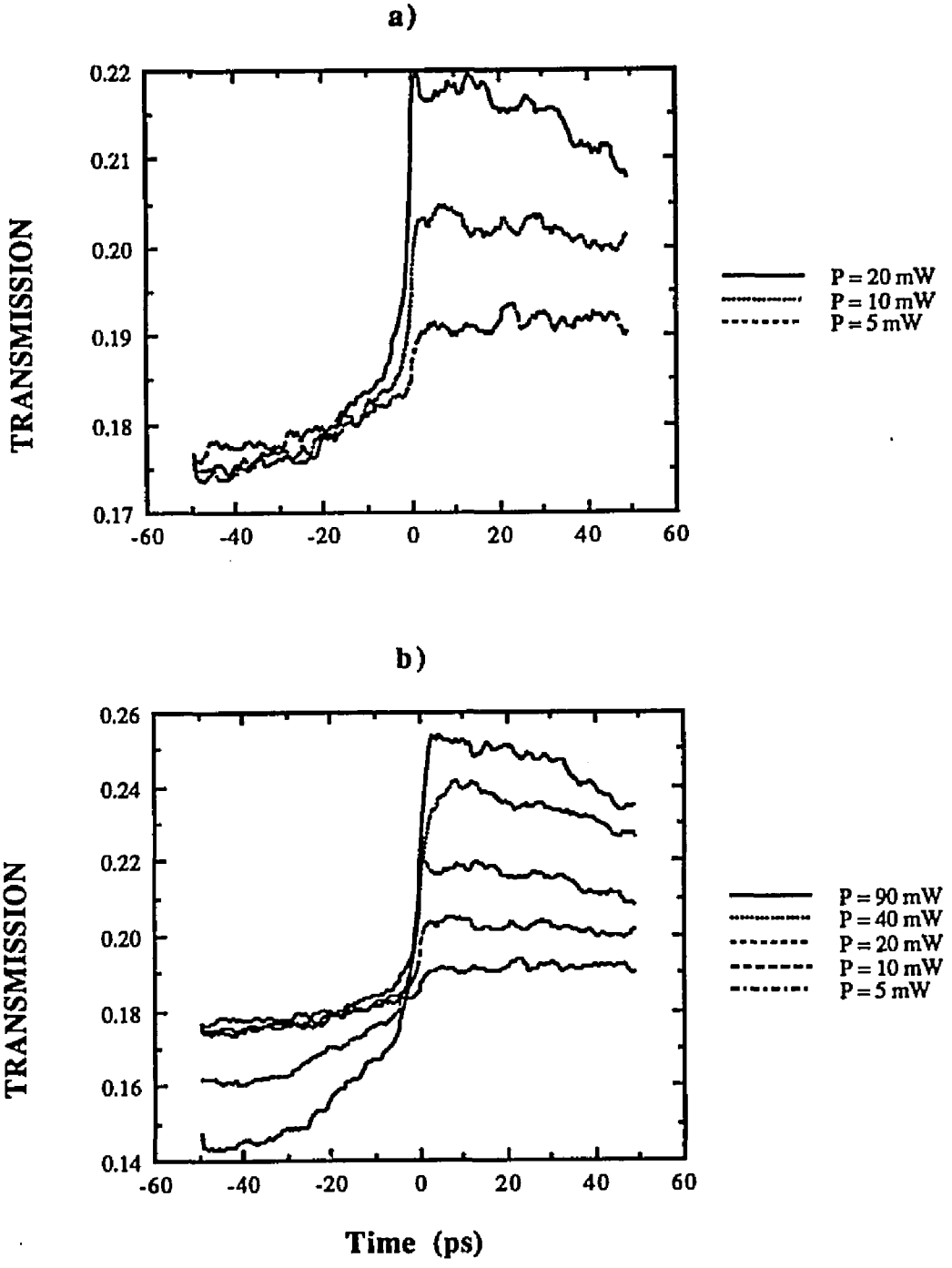

Figure 4.4 - Switching Characteristics for GaInAs Etalon.

a heating effect in the etalon. As the temperature increases, the Fabry-Perot fringe shifts to longer wavelength. Since the laser wavelength is positioned on the rising edge of a fringe, any wavelength shift, positive or negative, will change the transmission of the probe. In this case the fringe shifts to higher wavelengths, thus giving us a lower transmission of the probe for negative time delays.

The carrier recovery dynamics were measured using the same system described above except that the delay was changed to,-50 to +450 ps so that more data on the recovery side of the switching could be measured. Carrier lifetimes τ was estimated from the data, by using a curve fitting program that calculated the best fit to $e^{-t/\tau}$. Figure 4.5 (a) shows the recovery time for the 90 Å GaAlInAs MQW. The average from several measurements resulted in $\tau \simeq 750$ ps. For the 40 Å GaInAs MQW, we got $\tau \simeq 2.3$ ns as shown in Figure 4.5 (b). Figure 4.6 shows the switching recovery time $\tau \simeq 125$ ps for the GaInAs etalon. This result is an imporvement in recovery time of nearly 20 times that of the GaInAs MQW. Similar results of faster MQW etalon recovery as compared to the MQW sample were reported in GaAs [Lee et al. (1986)]. This improvement in recovery time could be due to the poorer quality of the MQWs in the etalon grown on top

of the $\lambda/4$ layers. For the etalon recovery measurements, it is desirable to look at more recovery data than is presented here. Total understanding the recovery response is not obvious from the data presented here.

Similar measurement of carrier lifetimes were made [Khitrova et al.(1991)]. Carrier lifetimes of 1.1 ns for GaAlInAs and 5.3 ns for GaInAs MQWs were reported. The large difference in carrier lifetime for GaInAs is explained by the following. The GaInAs MQW sample has a very long full carrier recovery time that approaches 10 ns. To accurately fit an exponential curve to the samples' carrier lifetime, data should be taken over the entire recovery event to ensure proper curve fitting. For the 2 ps measurements, data was taken only for the first .5 ns of the carrier lifetime which is only approximately 5% of the full carrier recovery time. Therefore the curve fitting program produces an inaccurate measurement of the carrier lifetime for the GAInAs MQW sample due to the small percentage of data as compared to the full recovery event. For the GaAlInAs MQW, the full recovery time is much less than in the GaInAs MQW, therefore, the .5 ns of data represents a larger portion of the carrier lifetime and accurate measurement of the lifetime are made by the curve fitting program.

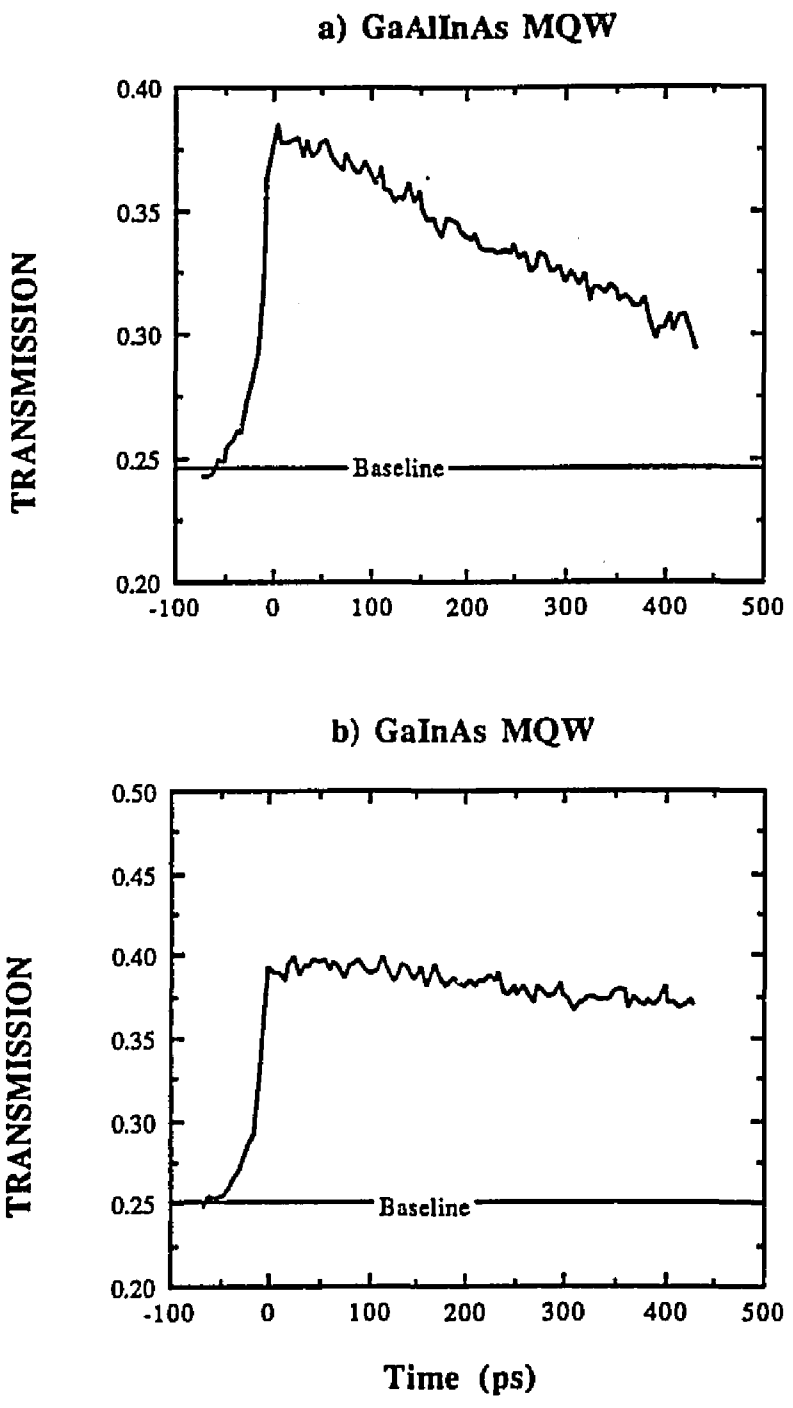

Figure 4.5 - Carrier Lifetimes for a) GaAlInAs and b) GaInAs.

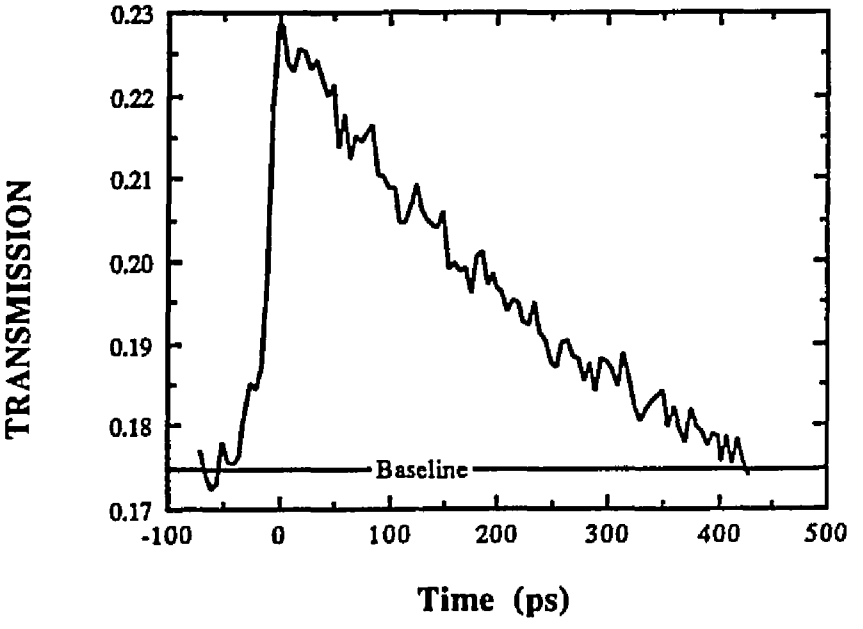

Figure 4.6 - Switching Recovery Time for a GaInAs Etalon.

4.2 Nanosecond Pulse Testing

The nonlinear absorption was measured using as pump-probe system in which the pump and probe pulses were coincident in time. In order to measure the nonlinear absorption spectrum, one needs a tunable laser source in the vicinity of the bandedge. Since dye laser technology does not exist at 1.3 μm, a system which utilizes frequency difference mixing was developed. The fundamental laser source used was a Spectron Q-Switched YAG Laser at 1.06 μm

with a 10 Hz rep-rate. Internal to the laser was a second harmonic generator, which was used to pump a dye laser system. The Rohdamine 6G dye laser source output was tunable between 568 - 594 nm. In order to produce tunable wavelengths needed at 1.3 μm, a $LiIO_3$ crystal was used to produce the difference frequency mixing between the dye and fundamental YAG. The result was a tunable infrared laser from 1.22 - 1.35 μm. This tunable source provided the means for measuring bandedge absorption spectra around the 1.3 μm region.

The pump-probe system utilized in this experiment used the 1.06 μm laser as the pump and the tunable IR laser for the probe. The Q-switched pulses at 1.06 μm contain high enough energy to saturate the excitons. By monitoring the transmission of the tunable IR beam, the exciton saturation can be measured. System parameters were 10 ns pulse width for the pump and 4 ns for the probe. Spot sizes diameters of 135 μm and 37 μm, for pump and probe were measured. The samples were mounted at Brewster's angle to minimize Fabry-Perot oscillations in the absorption spectrum. To monitor the transmission change in the probe a two detector system was used: The first detector measured a portion of the signal before the sample and was used as a reference signal. The second detector measured the transmitted signal through

the sample. Due to the frequency difference generation in the crystal, pump and probe beams were orthogonally polarized. By placing an analyzer in the path of the detected signal, the pump beam could be blocked and the probe beam could be detected. A boxcar averager was then used to collect the data and measure the transmission spectrum. The nonlinear absorption measurements were preformed by sweeping the wavelength of the tunable IR laser system for several different pump intensities. The relative transmission values for the samples were obtained from the ratios between the transmitted and the reference signals. The absolute transmission value for the samples was obtained from the ratio of the relative transmission with and without the sample. Figure 4.7 shows the room-temperature absorption spectrum for a)GaInAs and b)GaAlInAs MQWs. It can be seen that the heavy-hole exciton completely saturates for the highest pump powers. Table 4.2 lists the calculated carrier densities for each pump intensity as reported by [Hsu et al. (1991)]. The exciton saturation carrier density at the heavy-hole exciton peak was also determined by a best fit of the experimental data to a Lorentzian equation describing saturation. The reported saturation carrier densities were 1.2×10^{18} and 1.0×10^{18} cm^{-3} for GaInAs and GaAlInAs respectively.

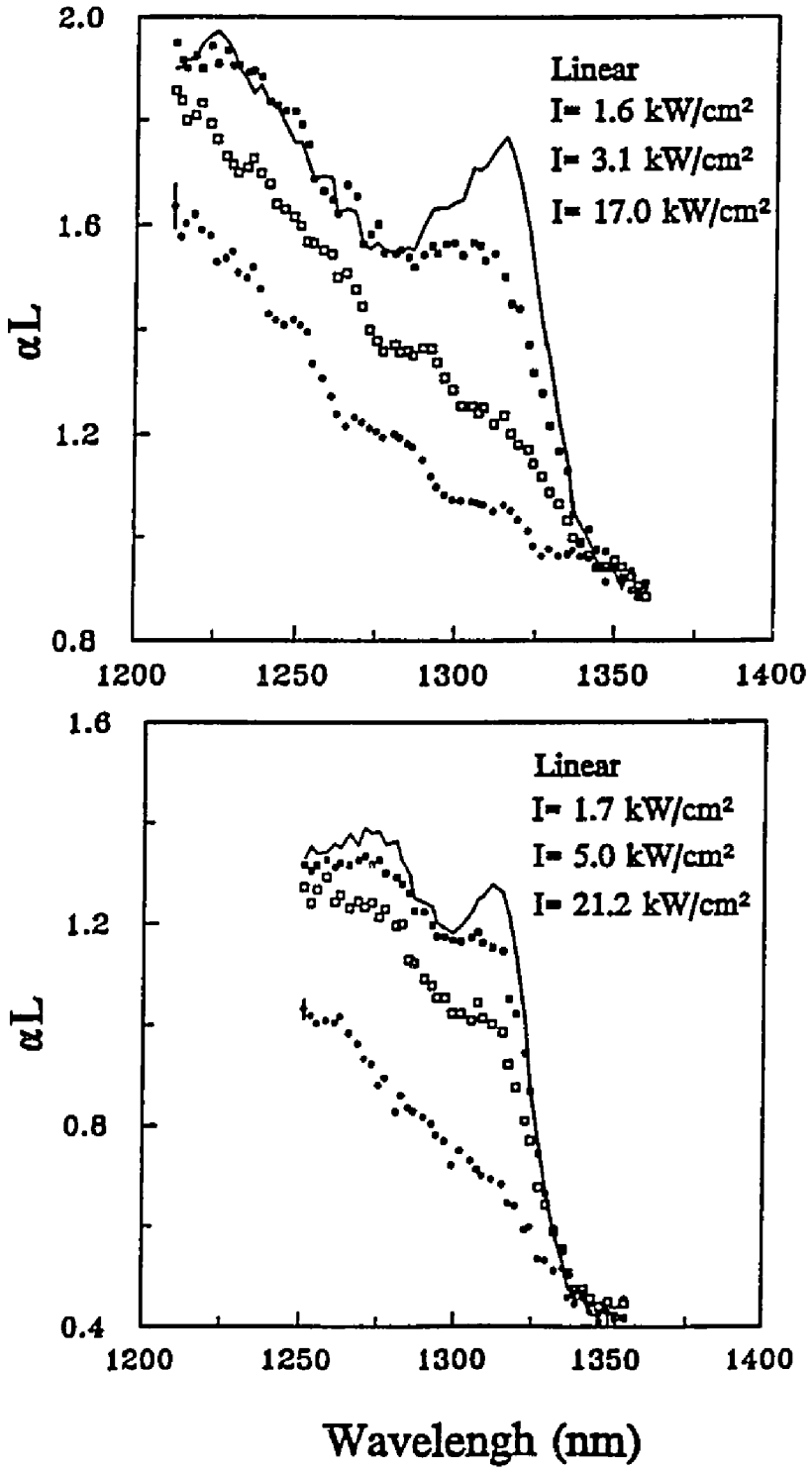

Figure 4.7 - Exciton Absorption Saturation in a) GaInAs and b) GaAlInAs MQWs.

- Table 4.2 - Exciton Saturation Densities and Photo Generated Carrier Densities. 45

GaInAs		GaAlInAs	
Pump Intensity	Carrier Density	Pump Intensity	Carrier Density
kW/cm^2	cm^{-3}	kW/cm^2	cm^{-3}
1.6	$6.4x10^{17}$	1.7	$2.1x10^{17}$
3.1	$1.2x10^{18}$	5.0	$6.2x10^{17}$
17.0	$6.7x10^{18}$	21.1	$2.6x10^{18}$

5.0 CONCLUSION AND DISCUSSION

In conclusion, we have presented the photo-induced optical characteristics of GaInAs/AlInAs and GaAlInAs/AlInAs MQWs at 1.3 μm. Saturation of the excitonic resonance in the nonlinear absorption spectrum have been observed for photo-generated carriers. Also a 20 fold decrease in switching recovery time has been seen in a GaInAs MQW etalon as compared to the carrier lifetime in the MQW sample.

Saturation densities for both MQW samples were approximately 1 x 10^{18} cm^{-3}. These results are close to the reported values for GaAs/AlGaAs MQWs. Carrier lifetimes for GaAlInAs were measured to be 750 picoseconds. In the GaInAs etalon, the switching recovery time was measured to be 125 picoseconds. This etalon also showed a pulse limited switching speed of approximately 5 picoseconds.

In an effort to increase the contrast ratio of the etalons, it has been proposed that asymmetric etalon be developed in GaInAs and GaAlInAs materials at 1.3 μm. It is expected that these types of structures could obtain contrast ratios on the order of a few hundred. Larger switching ratios would allow these devices to be integrated

into several optical communication test-beds where device and system performance could be measured.

A second technique proposed employs a fast excitonic absorption bleaching and recovery found in a "tunneling biquantum well" (BQW) structure. Picosecond switching and recovery were reported by [Tackeuchi et al. (1991)], from these BQW in GaAs. Growth of these structures with GaInAs or GaAlInAs could produce the fastest switching elements at 1.3 μm.

REFERENCES

Gibbs, H., Monthly Report, Rome Laboratories, 8 Aug. 1990.

Hsu, C.C., McGinnis, B.,Sokoloff, J.,Khitrova, G., Gibbs, H., Peyghambarian, N., Johns S. and Krol, M., to be published (1991)..

Khitrova, G., Iwabuchi, T. and Gibbs, H., Superlattices and Microstructures 8, 439 (1990).

Khitrova, G.,Iwabuchi, I.,Chuang, C.,Yoon T. and Gibbs, H., APL to be published (1991).

Khitrova, G., Iwabuchi, T., Chuang, C.L., Yoon, T., Pon, R. and Gibbs, H., CLOE May (1991).
Lambsdorff M., Kuhl, J., Rosenzweig, J., Axmann, A. and Schneider, J., APL 58(18), 29 April 1991.

Lee, Y., Gibbs, H., Jewell, J., Duffy, J., Venkatensan, T., Gossard, A., Wiegmann W. and English, J., APL 49(9), 1 Sep. 1986.

Migus, A., Antonetti, A., Hulin, D., Mysyrowicz, A., Gibbs, H., Peyghambarian N. and Jewell, J., APL 46(1), 1 Jan. 1985.

Park, S., Morhange, J., Jeffery, A., Morgan, R., Chavez-Pirson, A.,Gibbs, H., Koch, S., Peyghambarian, N., Derstine, M., Gossard, A., English, J. and Weigmann, W., APL 52(15), 11 April 1988.

Prucnal, P., Johns, S., Krol, M. and Stacy, J., OSA Boston Ma., Nov. 1990.

Silberberg, Y., Smith, P.,Miller, D.,Tell, B., Gossard, A. and W. Wiegmann, APL 46(8), 15 April 1985.

Sokoloff, J., Johns, S., Krol, M., Stacy, J., RADC-TR-90-389, Doc. 1990.

Tackeuchi, A., Muto, S., Inata, T. and Fujii, T., APL 58(15), 15 April 1991.

Tai, K., Jewell,J., Tsang,W., Temkin,H., Panish, M. and Twu, Y., APL 50(13), 30 March 1987.

Tucker, R., Eisenstein, G. and Koroyky, S., J. Lightwave Tech.,Vol.6 No. 11, Nov. 1988.